

Article

Not peer-reviewed version

Antibacterial and Photocatalytic Activity of ZnO/Au and ZnO/Ag Nanocomposites

[Mariana Busila](#)*, [Viorica Mușat](#), [Petrică Alexandru](#), [Cosmin Romanitan](#), [Oana Brincoveanu](#), [Vasilica Tucureanu](#), [Iuliana Mihalache](#), [Alina-Viorica Iancu](#), [Violeta Dediu](#)*

Posted Date: 27 October 2023

doi: 10.20944/preprints202310.1795.v1

Keywords: ZnO/Au; ZnO/Ag; nanocomposites; antimicrobial; photocatalytic activity



Preprints.org is a free multidiscipline platform providing preprint service that is dedicated to making early versions of research outputs permanently available and citable. Preprints posted at Preprints.org appear in Web of Science, Crossref, Google Scholar, Scilit, Europe PMC.

Copyright: This is an open access article distributed under the Creative Commons Attribution License which permits unrestricted use, distribution, and reproduction in any medium, provided the original work is properly cited.

Article

Antibacterial and Photocatalytic Activity of ZnO/Au and ZnO/Ag Nanocomposites

Mariana Busila ^{1,*}, Viorica Musat ¹, Petrică Alexandru ¹, Cosmin Romanitan ²,
Oana Brincoveanu ², Vasilica Tucureanu ², Iuliana Mihalache ², Alina Viorica Iancu ^{3,4}
and Violeta Dediu ^{2,*}

¹ Centre of Nanostructures and Functional Materials-CNMF, Engineering Faculty, "Dunarea de Jos" University of Galati, Domneasca Street 111, 800201, Galati, Romania

² National Research and Development Institute in Microtechnologies – IMT Bucharest, 126A Erou Iancu Nicolae Street, 077190, Bucharest, Romania

³ Department of Morphological and Functional Sciences, Faculty of Medicine and Pharmacy, "Dunărea de Jos" University, 800008 Galati, Romania

⁴ Medical Laboratory Department, Clinical Hospital for Infectious Diseases "Sf. Cuvioasa Parascheva", 800179 Galati, Romania

* Correspondence: mariana.busila@ugal.ro (M. Busila) & violeta.dediu@imt.ro (V. Dediu).

Abstract: The use of nanoparticles as antimicrobial agents can be one of the strategies to overcome the tendency of microbes to become resistant to antibiotics' action. In this study, two composites ZnO/Au and ZnO/Ag, having 1% wt. of noble metal content, were synthesized by simple aqueous solution methods. The structure and morphology of the resulting nanocomposites were analyzed by standard structural and optical characterization methods. The formation of Au NPs and Ag NPs in these experiments was also discussed. The antimicrobial properties of ZnO, ZnO/Au and ZnO/Ag nanomaterials were investigated against Gram-negative bacteria (*Pseudomonas aeruginosa*) and Gram-positive bacteria (*Staphylococcus aureus*). The electrostatic interaction between ZnO and noble metals nanoparticles have contributed to a better visible light adsorption, which led to an enhanced antimicrobial activity. The photocatalytic tests indicated an improvement in photocatalytic degradation of the methylene blue (MB) under UV irradiation using ZnO/Au and ZnO/Ag nanocomposites compared to bare ZnO. The introduction of noble metallic nanoparticles in ZnO matrix proved to be an effective strategy to increase their antimicrobial activity against *P. aeruginosa* and *S. aureus* and their photocatalytic activity evaluated through the degradation of MB dye. Comparing the enhancing effects of Au and Ag, it was found that ZnO/Au was a better antimicrobial agent while ZnO/Ag was more effective photocatalyst under UV irradiation.

Keywords: ZnO/Au; ZnO/Ag; nanocomposites; antimicrobial; photocatalytic activity

1. Introduction

During the last decades, engineered nanomaterials have been obtained and tested in new different applications (medicine [1], environment [2], energy [3], etc.). Synthesis methods have developed intensively so that a great variety of nanostructures were obtained [4]. Nanoparticles (NPs) have specific physical-chemical characteristics like high surface-to-volume ratio, high reactivity, and amenability to surface modification [5]. These properties recommend them for antimicrobial applications, being able to effectively target and kill Gram-positive and Gram-negative bacteria. Nowadays the accelerated spread of antibiotic resistance and the small number of new released antibiotics have caused a strong preoccupation to develop new strategies to defeat this public health threat [6]. NPs have already proven that they can be an alternative to classic antimicrobial agents being unlikely to induce antimicrobial resistance [7,8] although some forms of resistance in the case of Ag have been reported [9,10]. Although there is extensive research regarding the antibacterial mechanism of nanostructured materials is not fully elucidated [11], three plausible

routes were proposed (i) reactive oxygen species (ROS) generation, (ii) the release of metal ions in aqueous media, and (iii) electrostatic interaction with the cell wall.

Among antimicrobial nanomaterials, ZnO has been reported to exhibit broad-spectrum antibacterial properties against [12], viruses [13–15], and fungi [16,17] and is generally regarded as safe for humans. The interest towards ZnO was facilitated by the relative ease in synthesis of different kind of morphologies [9]. Nano-ZnO can act against bacteria mainly through ROS generation, where the electron–hole pairs generated by the light irradiation create free radicals which, consequently, destroy cellular constituents. The wide bandgap of ZnO determines a relatively low ROS production in the visible range, being more active in UV range. One approach aiming to extend the light absorption to the visible region is the coupling with plasmonic metals [18]. The formation of metal–semiconductor interface, the semiconductor's ability to absorb light in the visible range is improved and the recombination of photogenerated charge carriers is hindered, leading to the augmentation of ROS generation. Different ZnO/noble metal nanocomposites have been increasingly developed, mainly for photocatalytic applications [19,20]. The usage of these plasmonic nanocomposites against microbes is a hot topic [18] and research still needs to be undertaken to reach results that can be transferred into practical applications. Au and Ag can enhance the photocatalytic antimicrobial action of ZnO and they can also enhance the treatment efficiency due to their intrinsic antimicrobial activity [21]. In a previous study, we demonstrated that ZnO/Au nanocomposites, composed of small ZnO nanorods and small AuNPs work through a synergistic action proving to be more effective against *E. coli* and *S. aureus* than ZnO alone [22]. Comparing the two metals, AuNPs have the advantage of a high degree of stability and biocompatibility, while AgNPs have proved undeniable antimicrobial qualities. Hernández-Sierra et al. reported a comparative investigation of the bactericidal activity of Ag, ZnO, and Au nanoparticles on *Streptococcus mutans* (*S. mutans*) [23] and showed that Ag nanoparticles exhibited the most activity in controlling *S. mutans*, the main cause of dental caries. Ag NPs deposited on ZnO proved to have better biocompatibility than metallic nanoparticles while preserving their antimicrobial properties [24,25].

Another promising application of nano-ZnO is in photocatalysis, as eco-friendly and effective photoactive material that can degrade different recalcitrant organic compounds pollutants from wastewater [26]. The conventional wastewater treatment methods do not completely mineralize even after a long processing time. The key aspect in photodegradation processes over ZnO nanostructures is the utilization of photoexcited charge carriers to break down selected contaminants into non-toxic substances. Photocatalytic removal of organic compounds implies the adsorption of the organic pollutants on the surface of catalyst, oxidation and reduction reactions at interface, triggered under various light irradiations, resulting a complete mineralization of the pollutant. ZnO has emerged as one of the most preferable photocatalyst candidate because of its strong UV absorption, high initial activity rate, also it is safe for the environment and cheaper to produce than TiO₂. However, the practical application of ZnO is hindered due to its large band gap energy, being active mostly under UV irradiation, and due to the rapid recombination of the photoinduced electron–hole pairs, faster than the surface redox reactions [27]. One promising approach to modulate the absorption of ZnO and to overcome the rapid recombination of charge carriers is the coupling of noble metals with nano-ZnO [28–30], using the surface plasmon resonance properties of noble metals [8]. Au and Ag nanoparticles can extend the light absorption to the visible range and can prolong the lifetime of photogenerated electrons and holes. The Schottky barrier established at the metal–semiconductor interface can increase photocatalytic activity by preventing the recombination of photogenerated electron and holes, increasing the interfacial charge-transfer between noble metal and semiconductor and prolonging the carrier lifetime [31,32]. Upon modification with Au or Ag, the metal centers act as an electron sink/trap in ZnO, increasing the photocatalysis efficiency under visible and UV irradiation. The weak electrostatic interactions between noble metals and ZnO is the main challenge for the synthesis of nanocomposites with a good dispersion of metal nanoparticles in the oxide matrix. It is important to ensure the heterogeneous growth of noble metals nanoparticles on ZnO in order to create metal-ZnO heterojunctions. It was demonstrated that a small quantity of noble metals is needed to induce significant improvements in organic dyes degradation. Adding 1% Ag to a ZnO

photocatalyst coated microreactor lead to 91% degradation of methylene blue dye from water under UV-A irradiation for 2.5 minutes [33]. Other researchers found that a content of 1.5% of Ag NPs in nanocomposites is most favorable for maximizing the photocatalytic performances, and exceeding this percentage decreases the photodegradation efficiency [31]. Various Au/ZnO heterostructures with different gold content were reported as potential materials for photocatalysis. In reference [34] a 1.30 %Au content in ZnO/Au nanomaterial achieved the best performance in the degradation of methylene blue dye and was superior compared to the effect of silver on ZnO effectiveness. Other researchers found that, in fact, silver has a greater positive influence than gold in the efficiency of the photocatalytic degradation of Congo red dye under UV irradiation [29]. When employed as photocatalysts for methylene blue degradation, it was found that Au(3%)/ZnO exhibited superior performance than the pure ZnO [35].

In this study, we have synthesized ZnO/Au and ZnO/Ag nanocomposites, with 1%wt noble metal, through the reduction of Au or Ag salts using citric acid in the presence of commercial ZnO nanoparticles. The photocatalytic activity of the obtained nanomaterials was measured by the degradation of methylene blue (MB) cationic dye in an aqueous solution. Also, the antibacterial activity of these nanocomposites against *Pseudomonas aeruginosa* (*P. aeruginosa*) and *Staphylococcus aureus* (*S. aureus*) was studied under both light and dark conditions. The results showed a significant difference in the antibacterial activity of ZnO/Au and ZnO/Ag nanocomposites.

2. Results and Discussion

2.1. Characterization of the ZnO/Au and ZnO/Ag nanocomposites

To assess the structural features of the investigated samples, X-ray diffraction investigations were performed. Figure 1 presents the experimental XRD patterns, as well as the simulated data in the framework of the Rietveld refinement [38].

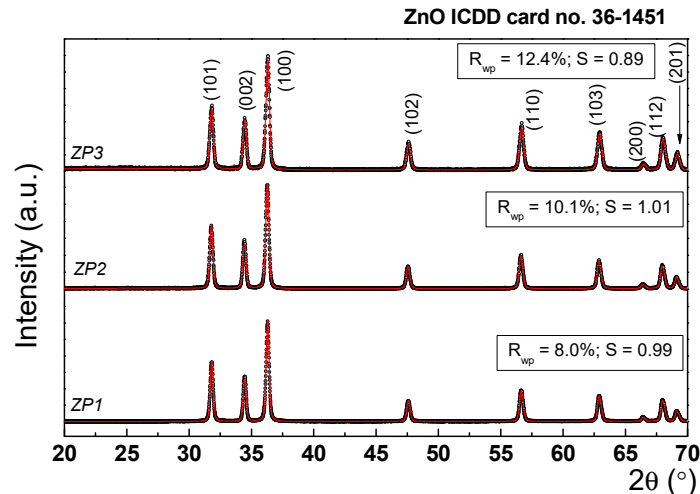


Figure 1. Experimental XRD patterns (black points) and simulated data in the framework of the Rietveld refinement (red line).

This refinement is based on the least squared method of the theoretical profile against the experimental XRD spectrum. Briefly, the principle of the refinement lies in the minimization of a function M which accounts for the difference between a calculated profile y_i^{calc} and the observed data y_i^{obs} , with the following form [39].:

$$M = \sum W_i \left\{ y_i^{obs} - \frac{1}{S} y_i^{calc} \right\}^2 \quad (4)$$

where W_i is the statistical weight and S is an overall scale factor such that $y_i^{calc} = S y_i^{obs}$. The values of the fitting parameters, R_{wp} (weighted parameter) and S (scale factor) are presented in Figure 1 and the goodness of the fits is proved by the reasonable value of these, i.e. $R_{wp} \sim 10\%$ and S

~ 1. The values for the unit cell parameters, crystallite size and lattice strain determined using Rietveld fit are listed in Table 2.

Table 2. Unit cell parameters, mean crystallite size, lattice strain and fitting parameters.

| Sample | Unit cell parameters (nm) | | Crystallite size (nm) | R _{wp} % | S | Lattice strain (%) |
|--------|---------------------------|------|-----------------------|-------------------|--------|--------------------|
| | a | c | | | | |
| ZP1 | 0.325 | 0.52 | 31.1 | 8.00 | 0.9933 | 0.73 |
| ZP2 | 0.325 | 0.52 | 27.5 | 10.12 | 0.9110 | 0.64 |
| ZP3 | 0.325 | 0.52 | 25.3 | 12.40 | 0.8935 | 0.42 |

As can be seen from Table 2, the ZnO unit cell parameters were not affected during AuNPs and AgNPs synthesis, preserving the wurtzit crystal structure of ZnO with a = b = 0.32 nm, and c = 0.52 nm. The crystallite size of the commercial ZnO sample (unmodified) is 23.2 nm and, after citrate functionalization this reaches to 31.1 nm. During the synthesis of AuNPs and AgNPs, the mean crystallite size of ZnO decreased to 27.5 nm in ZP2 and 25.3 nm in ZP3. This further implies an increase of the dislocation density (ρ), according to the following formula: $\rho \sim 1/\tau^2$, where τ is the mean crystallite size determined above [40]. At the same time, the lattice strain decreased from 0.73 to 0.42%, indicating a relaxation of the lattice simultaneously with the dislocation formation in the lattice. Overall, XRD analysis proved that the Au and Ag formation on ZnO NPs led only to small worsening of the crystal quality, by formation of dislocations in the ZnO lattice.

SEM micrographs of ZnO and composite samples are shown in Figure 2. As can be seen, ZnO particles appeared as polycrystalline small grains exhibiting diverse morphologies like: small rods, irregular parallelepipeds, and spheres, with a wide range of particle size distribution. Nanoparticles of different morphologies are well dispersed. The citrate used in the first stage of the composites' synthesis acts as a dispersant for commercial ZnO nanoparticles (that can be covered with organic stabilizers). Carboxylate anions attach to the positively charged surface of ZnO forming a Zn²⁺-citrate complex, kipping the ZnO NPs away from each other [41]. The elongated particles of commercial ZnO had a mean length of 131.6 +/-4.4 nm (N =150) and the spherical ones had a mean diameter of 43.1 +/-1.5 nm (N=250). During citrate functionalization, ZnO NPs undergo some morphological changes, especially in the case of aspherical particles, length of these nanoparticles increased-mean length being 199.5 +/-8.2 nm (N =150) while their diameter remains constant. Citrate ions were preferentially adsorbed on the positively charged zinc (001) plane, favouring the selective growth of the wurtzite crystal [42]. At the same time, the spherical NPs slightly decreased in diameter after the citric acid treatment to 41.1 +/-1.1 nm (N =250). Since SEM analysis technique cannot distinguish between ZnO, Au and Ag, the changes that appeared after the Ag and Au synthesis were highlighted through the statistical analysis of the nanoparticle's dimensions (Figure S1). In both nanocomposites, the number of particles with less than 50 nm in dimeters increases compared with those from the ZP1 sample. TEM analysis was performed on Au and Ag nanoparticles obtained in the absence of ZnO to bring additional information about the shape and dimensions of these nanoparticles. Therefore, Au NPs appear to be polycrystalline, near-spherical in shape with diameters ranging from 5 to 35 nm (inset of ZP2 SEM image - Figure 2) and for Ag NPs, these are rounder in shape with sizes between 8 and 40 nm (inset of ZP3 SEM image - Figure 2). Also, transmission electron micrographs show that gold nanoparticles are less polydisperse than Ag NPs, with most nanoparticles having around 30 nm in diameter. The EDS analysis has proven the presence of Au in ZP2 nanocomposite and of Ag in ZP3 sample (Figure 2) and the values are similar with those obtained from the ICP-OES analysis: Au content is 1.12 wt.% and, Ag is 0.97 wt.%. All the samples contain carbon from citrate groups, the amount being greater in both nanocomposites than in ZP1.

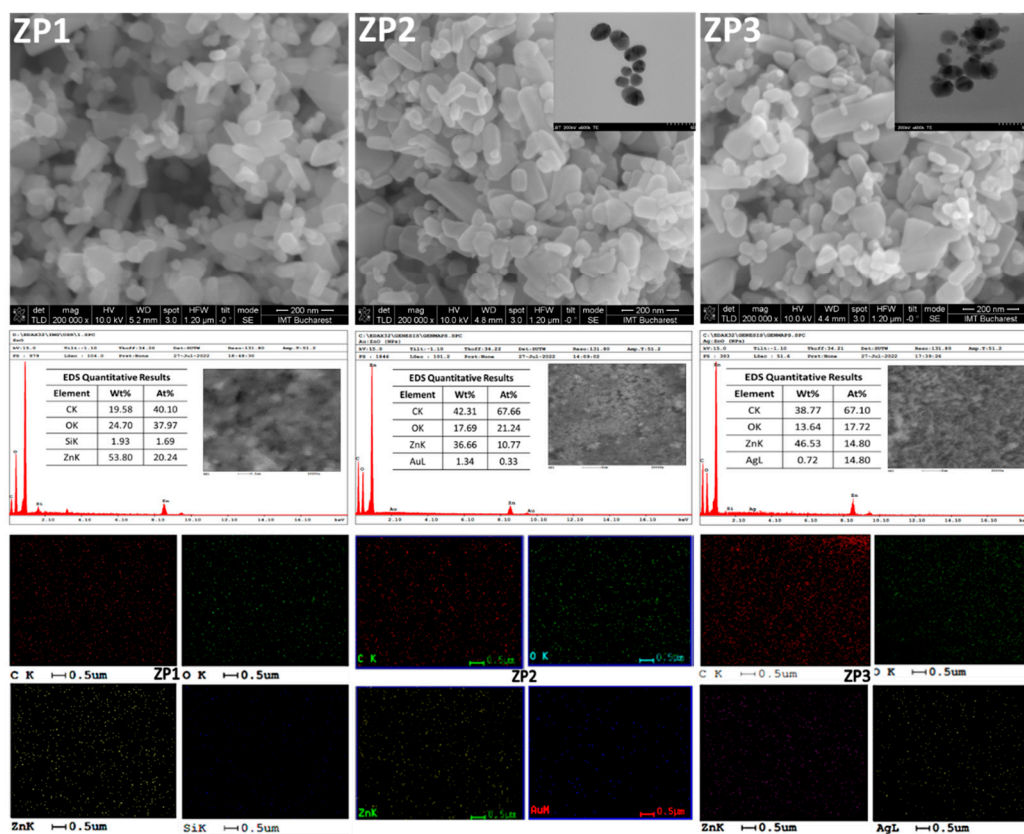
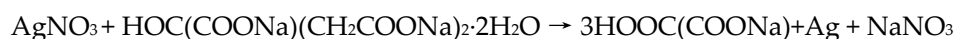
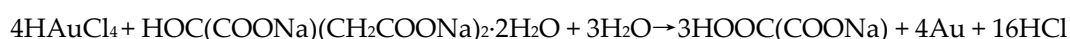


Figure 2. SEM micrographs, EDS elemental mapping of ZP, ZP2, and ZP3. The insets are TEM micrographs of Au NPs and Ag NPs.

During the synthesis of noble metal nanoparticles, ZnO nanocrystals act as seeding material for the nucleation of gold or silver nanocrystals [24]. Sodium citrate is used as a reducing agent for HAuCl_4 (precursor of Au NPs) and AgNO_3 (precursor of Ag NPs), respectively. The reduction reactions can be listed as the following [29]:



Also, the citrate groups perform a dispersant role, preventing the agglomeration of the newly synthesized Ag and Au nanoparticles [43].

The nature of the interactions that occur in the synthesis processes of nanocomposites and the newly formed bonds were evaluated through FTIR spectroscopy. Figure 3 presents spectra for commercial ZnO (ZP1) and the two nanocomposites (ZP2 and ZP3). All the spectra are characterized by absorption bands observed below 600 cm^{-1} which can be attributed to the vibrational mode of the Zn-O bonds in the wurtzite structure of ZnO [44].

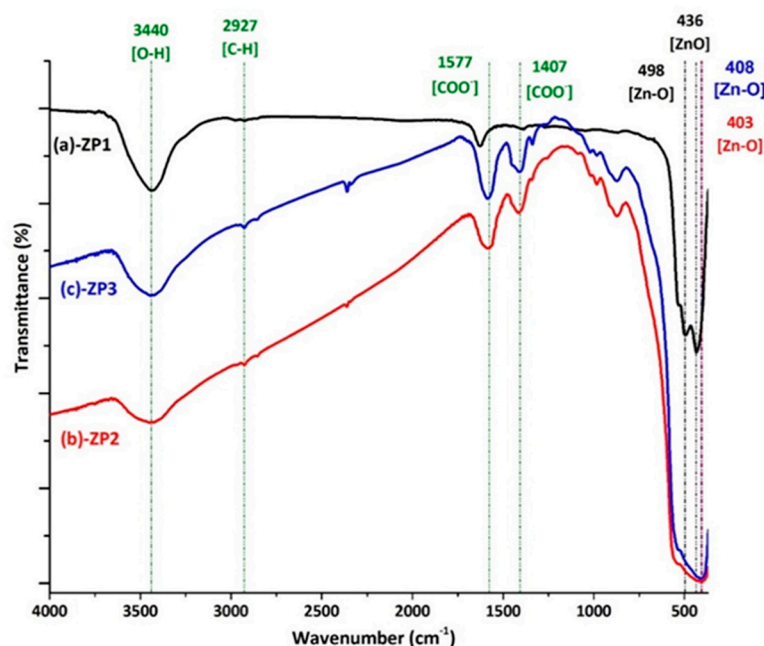


Figure 3. FTIR spectra for (a) ZP1, (b) ZP2, and (c) ZP3 samples.

In the case of the ZP1, three absorption peaks are associated with the vibration mode of the Zn-O bonds, suggesting the coexistence of particles with different sizes or a high agglomeration tendency. The peak centered at 439 cm^{-1} , corresponding to the E1 (TO) mode of hexagonal ZnO in the ZP1 spectrum, undergoes a slight shift towards lower wavenumbers in ZP2 and ZP3 due to the formation of nanocomposites. However, FTIR spectroscopy cannot detect specific bonds of Au or Ag atoms, suggesting the existence of an electrostatic interaction between the oxide and metallic particles. The broad band centered at about 3440 cm^{-1} corresponds to the stretching of the O-H bonds, indicating the presence of moisture in all samples. Besides these, in the spectral range 3000-600 cm^{-1} , peaks of different intensities associated with the process of synthesis and stabilization of nanoparticles can be observed, but without affecting the crystalline structure of ZnO, existing mainly near the surface of the oxide. The peaks associated with the mode of symmetric and asymmetric vibration of C-H bonds from saturated organic residues can be observed in the spectral range 3000-2800 cm^{-1} . The bands in the range 2400-2000 cm^{-1} indicate the presence of adsorbed CO_2 from the air on oxide nanoparticles. In the case of samples ZP2 and ZP3, the peaks in the range 1600-800 cm^{-1} are associated with the mode of vibration of the bonds from the trisodium citrate used with a double role in the synthesis process of metallic nanoparticles, both as a reducing and as a capping agent [45]. The bands in the 1580-1400 region can be associated with the symmetric and asymmetric vibration mode of the bonds from the COO^- group bonds in the citrate electrostatically attached to the nanoparticles.

2.2. Optical properties

The optical absorbance spectra (Figure 4a) showed strong absorption maximum located in the UV region and attributed to large excitonic binding energy, as expected for ZnO. Also, some modifications in the absorption spectra can be induced by the small increase in the ZnO particle size (seen in SEM images - Figure 3) which led to scattering of light, the decrease in crystallite size and lattice strain of wurtzite during nanocomposites synthesis (Table 2). For both nanocomposites, the absorption in visible range increased, more pronounced for ZnO/Au nanocomposites. The increase in optical absorption in visible range compared to ZP1 may occur due to the surface plasmon resonance absorption of silver nanoparticles (between 400-500 nm) and gold nanoparticles (between 500-700 nm), and that is evidence for ZnO-Au and ZnO-Ag interfaces existence. The stronger shift

in ZnO band position for ZnO/Au can be attributed to the higher electronegativity of gold when compared to silver, meaning that is more efficient in polling the electron density towards itself [46].

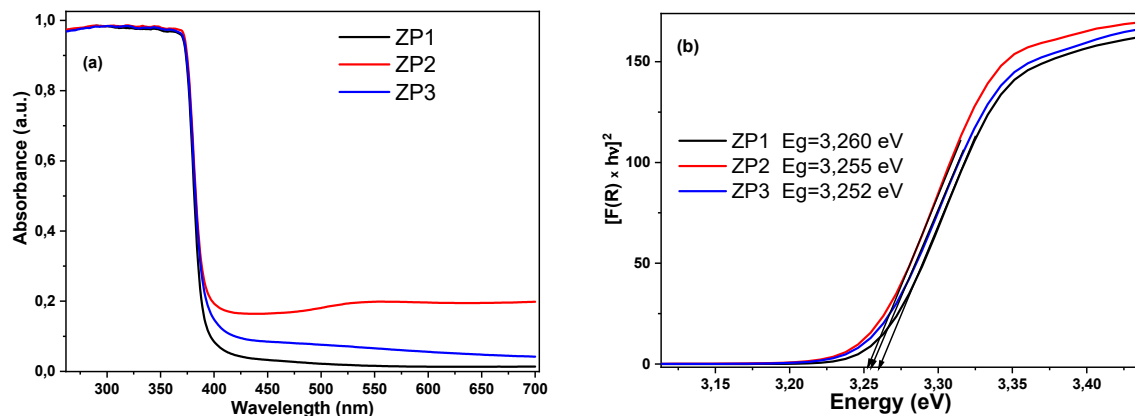


Figure 4. (a) UV-Vis optical absorbance and (b) Kubelka-Munk transformation for determination of direct energy band gap of ZP1; ZP2, and ZP3 samples.

The bandgap energies of the synthesized samples were determined by diffuse reflectance spectra (Figure 4b) [47], applying the equation (1). The results show a small yet detectable decrease in the energy band of nanocomposites, from 3.260 eV for ZP1 to 3.255 eV for ZnO/Au, and 3.252 eV for ZnO/Ag. This is due to the AgNPs and AuNPs electrostatic interactions with ZnO NPs, the decrease in the density of states and screening of the Coulomb interaction with a smaller surface-to-volume ratio. The decrease in the band-gap energy is in good agreement with the red shift observed in the absorbance spectra.

2.3. Antimicrobial activity

The results of disk diffusion method tests are presented in Table 3 and Figure 5. As can be observed, ZnO/Au and ZnO/Ag have a larger zone of bacterial growth inhibition compared to ZP1, for both Gram-positive and Gram-negative bacteria tested. The antibacterial efficiency shows a marked dependence on the chemical component of the material introduced into each agar disc. The size of inhibition zone of samples against *P. aeruginosa* was significantly larger, suggesting a better antimicrobial activity than that of samples against *S. aureus* bacteria. There is a difference in the appearance of the inhibition zone. The effect of the samples against *P. aeruginosa* bacteria can be bacteriostatic because the zone of inhibition is larger but more diffuse, while the zone of inhibition in the plate with *S. aureus*, even if it is smaller, is clear, which would suggest a bactericidal effect of all tested samples. In the case of *P. aeruginosa* strain, discs impregnated with citrate-ZnO nanoparticles (ZP1) have a diameter of the inhibition zone of 10 mm, ZnO/Au nanocomposite have a mean value of 18 mm, while ZnO/Ag nanoparticles the mean diameter of the inhibition zone is 13 mm. The same trend is observed in the case of the *S. aureus* strain, the ZP1 induced a inhibition zone of 9 mm, ZP2 a 14 mm IZ, while ZP3 the diameter of the inhibition zone was 12 mm.

Table 3. Mean zones of inhibition (in mm) produced by ZP1, ZP2 and ZP3 on the test bacteria.

| Sample | <i>Pseudomonas aeruginosa</i> (<i>P. aeruginosa</i>) | <i>Staphylococcus aureus</i> (<i>S. aureus</i>) |
|--------|---|--|
| ZP1 | 10 - diffuse | 9 - clear |
| ZP2 | 18 - diffuse | 9 – clear/14- diffuse |
| ZP3 | 13 - diffuse | 10 – clear/12 - diffuse |

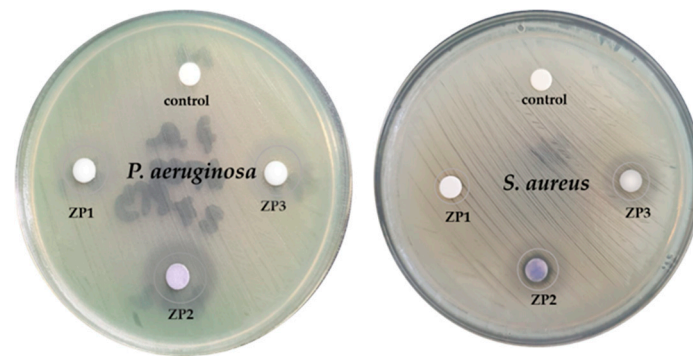


Figure 5. The zones of inhibition on MH agar plate on (a) *P. aeruginosa* and (b) *S. aureus*.

The release of cations from the nanoparticles is thought to be one of the mechanisms of antimicrobial action in the absence of the light. The interactions between ZnO, Ag, and Au nanoparticles and the bacterial membrane have been shown to be facilitated by the negatively charged molecules composing both Gram-positive and Gram-negative cell walls. These molecules have a great affinity for the generated positive ions. As a result, NPs are electrostatically attracted to the surface of bacteria, disrupting their cell walls and increasing their permeability. The dissimilarity in antimicrobial activity of nanocomposites is maybe due to the silver and gold distinct properties, silver has a higher reactivity, while gold is known for its chemical stability and corrosion resistance [48].

The results of MIC and MBC tests (Table 4) indicate that the planktonic cells of the Gram-positive strain *S. aureus* are more susceptible to citrate functionalized-ZnO, ZnO/Au and ZnO/Ag antimicrobial agents than the Gram-negative strains of *P. aeruginosa*. By measuring the effect of decreasing concentrations of nanomaterials on *S. aureus* bacteria growth over 24 hours, the MIC was found to be 6.25 $\mu\text{g/mL}$ (ZP1), 1.5 $\mu\text{g/mL}$ (ZP2), respectively 3.25 $\mu\text{g/mL}$ (ZP3), which are lower concentration values compared to that of the same nanoparticles against *P. aeruginosa* (12.5 $\mu\text{g/mL}$, 3.25 $\mu\text{g/mL}$, respectively 6.25 $\mu\text{g/mL}$). Similarly, the MBC for nanomaterials against *S. aureus* was found to be 6.25 $\mu\text{g/mL}$ (ZP1), 3.75 $\mu\text{g/mL}$ (ZP2), and 6.25 $\mu\text{g/mL}$ (ZP3), was lower in each case compared to the registered results against *P. aeruginosa* bacteria (25 $\mu\text{g/mL}$ (ZP1), 6.25 $\mu\text{g/mL}$ (ZP2), respectively 12.5 $\mu\text{g/mL}$ (ZP3).

Table 4. Minimum inhibitory concentration (MIC) and minimum bactericidal concentration (MBC) for ZP1, ZP2 and ZP3 on *P. aeruginosa* and *S. aureus*.

| Sample | <i>P. aeruginosa</i> | | MIC | MBC | <i>S. aureus</i> | | MIC | MBC |
|--------|----------------------|------|------|------|----------------------|------|------|------|
| | ($\mu\text{g/mL}$) | Obs. | | | ($\mu\text{g/mL}$) | Obs. | | |
| ZP1 | 50 | - | 12.5 | 25 | 50 | - | 6.25 | 6.25 |
| | 25 | - | | | 25 | - | | |
| | 12.5 | - | | | 12.5 | - | | |
| | 6.25 | + | | | 6.25 | - | | |
| | 3.75 | + | | | 3.75 | + | | |
| | 1.5 | + | | | 1.5 | + | | |
| ZP2 | 50 | - | 3.75 | 6.25 | 50 | - | 1.5 | 3.75 |
| | 25 | - | | | 25 | - | | |
| | 12.5 | - | | | 12.5 | - | | |
| | 6.25 | - | | | 6.25 | - | | |
| | 3.75 | - | | | 3.75 | - | | |
| | 1.5 | + | | | 1.5 | - | | |
| ZP3 | 50 | - | 6.25 | 12.5 | 50 | - | 3.75 | 6.25 |
| | 25 | - | | | 25 | - | | |
| | 12.5 | - | | | 12.5 | - | | |
| | 6.25 | - | | | 6.25 | - | | |
| | | | | | | | | |

| | | | |
|--|---|------|---|
| 3.75 | + | 3.75 | - |
| 1.5 | + | 1.5 | + |
| Positive (+): Turbidity indicating growth; Negative (-): No turbidity indicating absence of growth. | | | |

The difference in susceptibility may be attributed to variations in the cell surface characteristics between *P. aeruginosa* and *S. aureus* bacteria in particular in bacterial cell membrane [49]. Gram-negative bacteria have a periplasmic space that may act as a barrier, for the nanoparticles. Also, Gram-negative bacteria produce more proteins that bind to the surface of ZnO NPs making more difficult the interaction between the NPs and bacteria. Furthermore, Gram-negative bacteria exhibit an overexpression of efflux pumps and porins, that may limit the penetration of nanoparticles into the cell. In the case of *P. aeruginosa*, it has been observed that the bacterium produces a pigment called pyocyanin, which serves as a defense mechanism against nanoparticles [48,50]. Pyocyanin can interact with the ions produced or released by ZnO NPs or Ag NPs, thereby neutralizing their antimicrobial effects. These factors contribute to the higher susceptibility of Gram-positive *S. aureus* cells to ZnO NPs compared to Gram-negative *P. aeruginosa* cells.

The nanoparticles in contact with microbes interact with the bacterial cell membrane and starts to intervene into the basic processes of the cells. Among the results of nanoparticles actions, the most important are the damage of the bacterial cell membrane, cellular fluid leakage, DNA and protein disruption, and enzyme deactivation [51]. This interaction with bacteria is dependent on the chemical nature of the nanoparticles. Silver and gold have strong affinity to different chemical groups from the cell, particularly to SH-groups.–Ag-ions have proven that can block the respiratory chain, inhibiting the respiratory enzymes [21], disturb the replication of DNA, without inducing resistance to silver ions, although some studies have shown a few exceptions [52]. Compared to silver and ZnO, Au NPs have not been as extensively explored for their antibacterial properties, but now has become a hot research topic [53]. Small gold nanoparticles can perforate the bacterial cell membrane, which results in cell death [54] or can cause the depolarization of membrane potential and significant DNA damage causing apoptotic-like death [55]. From the literature, ZnO-based nanoparticles, doped or in conjugation with noble metals, have demonstrated effective antibacterial activity through the formation of ROS (especially OH and singlet oxygen radicals [56]) and the releasing of Zn²⁺ [57], responsible for the cellular damage. Furthermore, the citrate groups present in each synthesized nanomaterial contributed to overall antimicrobial effect [24].

2.4. Photocatalytic activity

The photocatalytic activities of the citrate-ZnO, ZnO/Au and ZnO/Ag nanocomposites were assessed by the degradation of MB under UV irradiation. Figure 6a shows the absorption spectra of the aqueous solution of MB with 40 mg of ZnO, ZnO/Au, and ZnO/Ag nano-photocatalysts. In the absence of ZP samples, the concentration of MB did not significantly decrease (1.14% MB degradation) under UV irradiation (Figure 6b). When using ZP1 as photocatalyst the concentration of MB decreased over the irradiation time, which can be attributed to nanometric dimensions. In the case of nanocomposite photocatalysts, the MB degradation capability is increased in comparison with that caused by bare ZnO NPs, proving that the presence of Au NPs or Ag NPs has a positive effect on the photocatalytic performance. According to experimental results, the calculated photocatalytic degradation efficiencies were 94.85% for ZP2 and 97.80% (ZP3), while for ZP1 achieved 83.12% (Figure 6b). The degradation rate of MB is higher in the case of nanocomposites compared to ZP1, proven by the higher slope of the ZP2 and ZP3 curves in Figure 6b. The increased photocatalytic effectiveness of the ZnO/Au and ZnO/Ag nanocomposites can be attributed to the synergetic effect of the nanocomposite’s constituents and to the specific charge-transfer at constituents’ contact. The strong electronic interaction between Au NPs and ZnO, and between Ag NPs and ZnO, respectively, facilitates the charge transfer from ZnO to noble metal nanoparticles, leading to a better charge separation of the photogenerated electron–hole pairs. The presence of noble metals in ZnO based nanocomposites can result in a decrease in work functions leading to a significant increase in electron

transfer rate and a faster rate of dye degradation [32]. In photocatalysis the charge carriers who have escaped annihilation migrate to the surface of the catalyst and initiate reactions with the surface adsorbed species. The holes react with H_2O molecules producing hydroxyl radicals, whereas the electrons react with dissolved oxygen resulting superoxide radicals or hydroperoxide radicals. All these species contribute to the degradation of methylene blue dye [58].

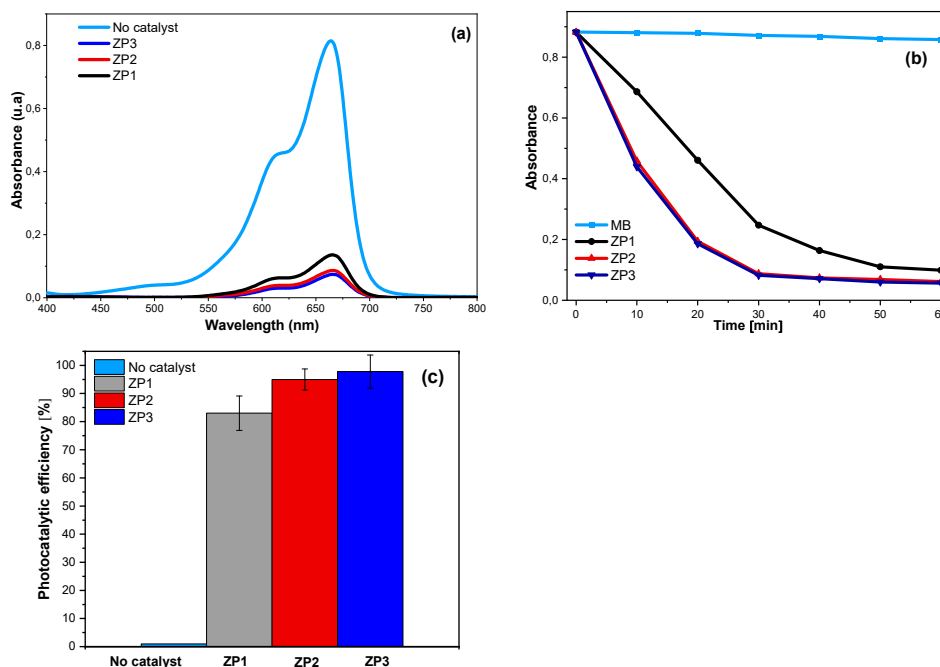


Figure 6. (a) The absorption spectra of MB solutions in the presence of ZP1, ZP2 and ZP3 samples -40 mg ZP/20 mg MB, after 1h of UV irradiation, (b) change in MB concentration with irradiation time, and (c) Photocatalytic efficiency of ZP1, ZP2 and ZP3 samples against MB (40 mg ZP/20 mg MB 1h of UV irradiation).

The photocatalytic efficiency of ZnO/Ag, a little higher than that of ZnO/Au is in concordance with the values of band gaps (Figure 4b). Other authors obtain a better improvement in removal of Red Congo dye under the UV light irradiation when Au NPs were deposited on ZnO compared to AgNPs deposition [29]. Fageria et al. [46] found that Au decorated ZnO exhibits a better photocatalytic efficiency in comparison with ZnO/Ag putting this result on account of the greater work function value of gold compared to that of silver.

3. Materials and Methods

3.1. Reagents

ZnO nanoparticles (<100 nm) were purchased by Merck (Darmstadt, Germany). Au (III) chloride trihydrate $\text{HAuCl}_4 \cdot 3\text{H}_2\text{O}$ (99%), silver nitrate AgNO_3 (99.999%), sodium citrate $\text{C}_6\text{H}_5\text{Na}_3\text{O}_7$ (99.0%), and Muller-Hinton Agar were purchased from Sigma-Aldrich and used without further purification.

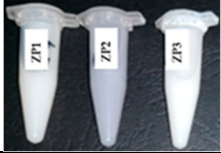
3.2. Preparation of ZnO/Au and ZnO/Ag nanocomposites

During nanocomposites synthesis, commercial ZnO NPs were firstly functionalized with citrate and then nanoparticles of Au or Ag were synthesized in the presence of citrate-functionalized ZnO NPs. 500 mg of commercial ZnO nanoparticles were dispersed in 100 ml of deionized water at room temperature using an ultrasonic bath for 30 min. In this dispersion, sodium citrate powder (0.7 mM) was added and maintained for 24 hours under magnetic stirring. Precursor powder of HAuCl_4 or AgNO_3 was added into the mixture followed by magnetic stirring for 2 hours in the dark. The resulting precipitate was centrifuged at 10,000 rpm washed with deionized water 4 times and dried

in an oven at 70 °C. The obtained ZnO/Au powder had a faint purple color while ZnO/Ag was light-yellow. For comparison, ZnO NPs functionalized with citrate were washed and dried. The samples were coded according to the Table 1.

Table 1. The samples code.

| Sample code | Nanomaterials |
|-------------|--------------------------------|
| ZP1 | Citrate functionalized-ZnO NPs |
| ZP2 | ZnO NPs/ Au NPs |
| ZP3 | ZnO NPs /Ag NPs |



3.3. Characterisation Techniques

X-ray diffraction investigations were done using a 9kW Rigaku SmartLab diffractometer ($\lambda_{\text{CuK}\alpha 1}$ = 0.154 nm) in parallel-beam configuration. Powder X-ray diffraction (PXRD) investigations were performed in $\theta/2\theta$ mode. The morphological features of samples were studied using a Quanta Inspect F scanning electron microscope (FEI Company) and their chemical composition was by energy dispersive X-ray spectroscopy (EDX). Fourier Bruker Optics Tensor 27 spectrometer was used to perform Transform Infrared (FTIR) spectroscopy to study the chemical bond configuration by averaging 64 scans with a resolution of 4 cm^{-1} , at room temperature, using the potassium bromide pellet method. The sizing of the ZnO nanoparticles and synthesized composite powders was performed using ImageJ software. The optical absorbance spectra of the powders were recorded at room temperature using Cary 5000 spectrophotometer (Agilent Technology). The diffuse reflectance spectra were recorded from 200 to 700 nm by 1 nm intervals. All spectra were baseline corrected with 100% R baseline collected over the same spectral domain using a white polytetrafluoroethylene standard sample. The band gap energy, E_g , was estimated from the Kubelka-Munk function $F(R)$ defined by the equation [1]:

$$K/S = (1-R)^2/2R \tag{1}$$

where K and S are the K-M absorption and scattering coefficients, and R is the reflectance. The K-M function was employed to determine the band gap energy (E_g) of the ZnO powders by replacing the optical absorption coefficient α in the analogous Tauc plots:

$$\alpha h\nu = A (h\nu - E_g)^n \tag{2}$$

where A is a constant, $h\nu$ is the incident photon energy, and the exponent $n = 1/2$ and 2 for direct allowed transition and indirect allowed transitions, respectively.

3.4. Antibacterial testing

3.4.1. Antibacterial susceptibility

Antibacterial susceptibility testing was determined using the Kirby-Bauer disk diffusimetric method on a standardized Mueller Hinton culture medium. *S. aureus* (ATCC25923) and *P. aeruginosa* (ATCC27853) were used as representative strains of Gram-negative and Gram-positive bacteria, according to the Clinical and Laboratory Standards Institute (CLSI) and the European Committee on Antimicrobial Susceptibility Testing (EUCAST) [36,37]. The bacterial inoculum was prepared by suspending 3-5 colonies in physiological serum. Turbidity of 0.5 on the Mac Farland scale (0.5 McFarland = 1.5×10^8 cells per mL) was measured by a nephelometer. Sterile paper discs (6 mm in diameter) were impregnated with 30 μL of an antimicrobial agent (30 mg/mL) and placed on agar plate with bacterial inoculum. After 15 minutes, the plates were placed in the thermostat at 35 °C in aerobiosis, for 24 hours. The sizes of the bacterial growth inhibition zone were measured in millimeters (mm). Each test was performed in triplicate and the average of the values was calculated.

3.4.2. Minimum inhibitory concentration (MIC) and minimum bactericidal concentration (MBC) assays

The MIC determination was performed by a microdilution method in according to the protocol M7-A10 of the Clinical and Laboratory Standards Institute (CLSI) [31] using a standardized Mueller-Hinton medium. Dispersions 100 µg/mL of all nanomaterials in dimethylsulfoxide (DMSO) were prepared and serial dilution, giving concentrations of 50, 25, 12.5, 6.25, 3.75, 1.5 µg/mL. The microplates were incubated at 37 °C for 24 h. Afterwards, it was established the concentrations at which tested nanomaterials inhibit growth of (MIC) or completely kill (MBC) *S. aureus* (ATCC25923) and *P. aeruginosa* (ATCC27853). All experiments were performed in triplicate and the results represent the average of the three measurements.

3.5. Photocatalytic testing

The assessment of photocatalytic activities was performed by the degradation of methylene blue (MB) dye in the presence of the synthesized samples, under UV irradiation (254 nm) from a mercury UV lamp at 100 KW. 40 mg of each photocatalysts were dispersed in 40 ml aqueous solution of MB (0.5 mg/mL). Before UV exposure, the suspension was stirred (at 800 rpm) for 30 min in the dark to reach an adsorption-desorption equilibrium. The temperature of the photooxidation reaction was maintained at 25 °C. At a regular irradiation time interval, the MB content was quantified by measuring the absorbance using the UV-vis spectroscopy using a Micro-plate reader with fluorescence spectrometer Infinite 200 PRO NanoQuant (Tecan, Switzerland). The efficiency of dye degradation was calculated using the relation:

$$\eta = \frac{A_0 - A_t}{A_0} \cdot 100 \quad (3)$$

where: A_0 is the the initial absorbance, and A_t is the at time 't'.

4. Conclusions

In this study ZnO/Au and ZnO/Ag nanocomposites were synthesized starting from commercial ZnO nanoparticles, which were functionalized with citrate, then Au or Ag nanoparticles dispersed between ZnO nanoparticles were obtained by citrate reduction method. The XRD and SEM analysis showed the ZnO/Au and ZnO/Ag crystalline structures and morphologies. FTIR spectroscopy confirms the formation of ZnO/Au and ZnO/Ag nanocomposites where metallic nanoparticles and ZnO NPs interact electrostatically. The effects of Au and Ag nanoparticles on the photocatalytic and light absorption of ZnO were investigated. Both noble metals improved the overall photocatalytic degradation efficiency of MB dye. The differences in the activities of AuNPs and AgNPs may be related to the in the in their work functions. The results of these studies demonstrate that introducing Au and Ag nanoparticle in contact with nano-ZnO, can delay significantly the recombination process of the photogenerated electron-hole pairs. The investigations showed that the combination of nano-ZnO with gold or silver nanoparticles (1%wt.) can lead to a significant improvement in the antimicrobial and photocatalytic activity of the ZnO.

Supplementary Materials: The following supporting information can be downloaded at the website of this paper posted on Preprints.org.

Author Contributions: Conceptualisation: V.D., M.B. and V.M.; writing: V.D., M.B., V.T., I.M, and C.R.; methodology M.B. and V.D; formal analysis, P.A., C.R., V.T., O.B., A.V.I., and I.M.; writing—original draft preparation V.D.; supervision, V.M.; funding acquisition V.D. and M.B. All authors have read and agreed to the published version of the manuscript.

Funding: This research was funded by the Core Program within the National Research, Development and Innovation Plan, 2022–2027, with the support of MCID, project no. PN 2370103 -8N/2023 and “Support and development of CDI-TT activities in the “Dunărea de Jos” University of Galati—Internal grant RF3639/30.09.2021.

Institutional Review Board Statement: This study did not require ethical approval.

Informed Consent Statement: Not applicable.

Data Availability Statement: No new data were created.

Conflicts of Interest: The authors declare no conflict of interest. The funders had no role in the design of the study; in the collection, analyses, or interpretation of data; in the writing of the manuscript; or in the decision to publish the results.

References

1. Pelaz, B.; Alexiou, C.; Alvarez-Puebla, R.A.; Alves, F.; Andrews, A.M.; Ashraf, S.; Balogh, L.P.; Ballerini, L.; Bestetti, A.; Brendel, C. Diverse applications of nanomedicine. *ACS nano* **2017**, *11*, 2313-2381.
2. Hasnat, M.A.; Hossain, M.I.; Ahsan, M.; Islam, M.F. Recent Developments in the Utilization of Nanomaterials for Sensing Platforms. *Recent Developments in Green Electrochemical Sensors: Design, Performance, and Applications* **2023**, 61-99.
3. Kumar, R.; Kumar, M.; Luthra, G. Fundamental approaches and applications of nanotechnology: A mini review. *Materials Today: Proceedings* **2023**.
4. Xia, Y.; Xiong, Y.; Lim, B.; Skrabalak, S.E. Shape-controlled synthesis of metal nanocrystals: simple chemistry meets complex physics? *Angewandte Chemie International Edition* **2009**, *48*, 60-103.
5. Behzadi, S.; Serpooshan, V.; Tao, W.; Hamaly, M.A.; Alkawareek, M.Y.; Dreaden, E.C.; Brown, D.; Alkilany, A.M.; Farokhzad, O.C.; Mahmoudi, M. Cellular uptake of nanoparticles: journey inside the cell. *Chemical society reviews* **2017**, *46*, 4218-4244.
6. Hetta, H.F.; Ramadan, Y.N.; Al-Harbi, A.I.; A. Ahmed, E.; Battah, B.; Abd Allah, N.H.; Zanetti, S.; Donadu, M.G. Nanotechnology as a Promising Approach to Combat Multidrug Resistant Bacteria: A Comprehensive Review and Future Perspectives. *Biomedicines* **2023**, *11*, 413.
7. Zhao, Y.; Chen, L.; Wang, Y.; Song, X.; Li, K.; Yan, X.; Yu, L.; He, Z. Nanomaterial-based strategies in antimicrobial applications: Progress and perspectives. *Nano Research* **2021**, 1-25.
8. Dediu, V.; Ghitman, J.; Gradisteanu Pircalabioru, G.; Chan, K.H.; Iliescu, F.S.; Iliescu, C. Trends in Photothermal Nanostructures for Antimicrobial Applications. *International Journal of Molecular Sciences* **2023**, *24*, 9375.
9. Hosny, A.E.-D.M.; Rasmy, S.A.; Aboul-Magd, D.S.; Kashef, M.T.; El-Bazza, Z.E. The increasing threat of silver-resistance in clinical isolates from wounds and burns. *Infection and drug resistance* **2019**, 1985-2001.
10. Wu, Z.; Chan, B.; Low, J.; Chu, J.J.H.; Hey, H.W.D.; Tay, A. Microbial resistance to nanotechnologies: An important but understudied consideration using antimicrobial nanotechnologies in orthopaedic implants. *Bioactive Materials* **2022**.
11. Shaikh, S.; Nazam, N.; Rizvi, S.M.D.; Ahmad, K.; Baig, M.H.; Lee, E.J.; Choi, I. Mechanistic insights into the antimicrobial actions of metallic nanoparticles and their implications for multidrug resistance. *International journal of molecular sciences* **2019**, *20*, 2468.
12. Kumar, R.; Umar, A.; Kumar, G.; Nalwa, H.S. Antimicrobial properties of ZnO nanomaterials: A review. *Ceramics International* **2017**, *43*, 3940-3961.
13. Karagoz, S.; Kiremitler, N.B.; Sarp, G.; Pekdemir, S.; Salem, S.; Goksu, A.G.; Onses, M.S.; Sozdutmaz, I.; Sahmetlioglu, E.; Ozkara, E.S. Antibacterial, antiviral, and self-cleaning mats with sensing capabilities based on electrospun nanofibers decorated with ZnO nanorods and Ag nanoparticles for protective clothing applications. *ACS Applied Materials & Interfaces* **2021**, *13*, 5678-5690.
14. Gupta, J.; Irfan, M.; Ramgir, N.; Muthe, K.; Debnath, A.; Ansari, S.; Gandhi, J.; Ranjith-Kumar, C.; Surjit, M. Antiviral Activity of Zinc Oxide Nanoparticles and Tetrapods Against the Hepatitis E and Hepatitis C Viruses. *Frontiers in Microbiology* **2022**, 13.
15. Melk, M.M.; El-Hawary, S.S.; Melek, F.R.; Saleh, D.O.; Ali, O.M.; El Raey, M.A.; Selim, N.M. Antiviral activity of zinc oxide nanoparticles mediated by plumbago indica L. Extract against herpes simplex virus type 1 (HSV-1). *International Journal of Nanomedicine* **2021**, *16*, 8221.
16. Lipovsky, A.; Nitzan, Y.; Gedanken, A.; Lubart, R. Antifungal activity of ZnO nanoparticles—the role of ROS mediated cell injury. *Nanotechnology* **2011**, *22*, 105101.
17. Kumar, R.S.; Dananjaya, S.; De Zoysa, M.; Yang, M. Enhanced antifungal activity of Ni-doped ZnO nanostructures under dark conditions. *RSC advances* **2016**, *6*, 108468-108476.

18. Marín-Caba, L.; Bodelón, G.; Negrín-Montecelo, Y.; Correa-Duarte, M.A. Sunlight-sensitive plasmonic nanostructured composites as photocatalytic coating with antibacterial properties. *Advanced Functional Materials* **2021**, *31*, 2105807.
19. Lu, J.; Wang, H.; Peng, D.; Chen, T.; Dong, S.; Chang, Y. Synthesis and properties of Au/ZnO nanorods as a plasmonic photocatalyst. *Physica E: Low-dimensional Systems and Nanostructures* **2016**, *78*, 41-48.
20. Kavitha, R.; Kumar, S.G. A review on plasmonic Au-ZnO heterojunction photocatalysts: Preparation, modifications and related charge carrier dynamics. *Materials Science in Semiconductor Processing* **2019**, *93*, 59-91.
21. Balestri, A.; Cardellini, J.; Berti, D. Gold and Silver Nanoparticles as Tools to Combat Multidrug-Resistant Pathogens. *Current Opinion in Colloid & Interface Science* **2023**, 101710.
22. Dediu, V.; Busila, M.; Tucureanu, V.; Bucur, F.I.; Iliescu, F.S.; Brincoveanu, O.; Iliescu, C. Synthesis of ZnO/Au nanocomposite for antibacterial applications. *Nanomaterials* **2022**, *12*, 3832.
23. Hernández-Sierra, J.F.; Ruiz, F.; Pena, D.C.C.; Martínez-Gutiérrez, F.; Martínez, A.E.; Guillén, A.d.J.P.; Tapia-Pérez, H.; Castañón, G.M. The antimicrobial sensitivity of Streptococcus mutans to nanoparticles of silver, zinc oxide, and gold. *Nanomedicine: Nanotechnology, Biology and Medicine* **2008**, *4*, 237-240.
24. Burlibaşa, L.; Chifiriuc, M.C.; Lungu, M.V.; Lungulescu, E.M.; Mitrea, S.; Sbarcea, G.; Popa, M.; Măruţescu, L.; Constantin, N.; Bleotu, C. Synthesis, physico-chemical characterization, antimicrobial activity and toxicological features of AgZnO nanoparticles. *Arabian Journal of Chemistry* **2020**, *13*, 4180-4197.
25. Mousavi-Kouhi, S.M.; Beyk-Khormizi, A.; Amiri, M.S.; Mashreghi, M.; Yazdi, M.E.T. Silver-zinc oxide nanocomposite: From synthesis to antimicrobial and anticancer properties. *Ceramics International* **2021**, *47*, 21490-21497.
26. Ong, C.B.; Ng, L.Y.; Mohammad, A.W. A review of ZnO nanoparticles as solar photocatalysts: Synthesis, mechanisms and applications. *Renewable and Sustainable Energy Reviews* **2018**, *81*, 536-551.
27. Zhang, X.; Chen, Y.L.; Liu, R.-S.; Tsai, D.P. Plasmonic photocatalysis. *Reports on Progress in Physics* **2013**, *76*, 046401.
28. Deng, Q.; Duan, X.; Ng, D.H.; Tang, H.; Yang, Y.; Kong, M.; Wu, Z.; Cai, W.; Wang, G. Ag nanoparticle decorated nanoporous ZnO microrods and their enhanced photocatalytic activities. *ACS Applied Materials & Interfaces* **2012**, *4*, 6030-6037.
29. Güy, N.; Özacar, M. The influence of noble metals on photocatalytic activity of ZnO for Congo red degradation. *International journal of hydrogen energy* **2016**, *41*, 20100-20112.
30. Putri, A.E.; Roza, L.; Budi, S.; Umar, A.A.; Fauzia, V. Tuning the photocatalytic activity of nanocomposite ZnO nanorods by shape-controlling the bimetallic AuAg nanoparticles. *Applied Surface Science* **2021**, 147847.
31. Sun, F.; Tan, F.; Wang, W.; Qiao, X.; Qiu, X. Facile synthesis of Ag/ZnO heterostructure nanocrystals with enhanced photocatalytic performance. *Materials Research Bulletin* **2012**, *47*, 3357-3361.
32. Ibănescu, M.; Muşat, V.; Textor, T.; Badilita, V.; Mahltig, B. Photocatalytic and antimicrobial Ag/ZnO nanocomposites for functionalization of textile fabrics. *Journal of Alloys and Compounds* **2014**, *610*, 244-249.
33. Akman, B.; Aras, O. Usability, durability and regeneration of Ag/ZnO coated microreactor for photocatalytic degradation of methylene blue. *Journal of Molecular Structure* **2022**, 1251, 132003.
34. Lin, W.-H.; Chiu, Y.-H.; Shao, P.-W.; Hsu, Y.-J. Metal-particle-decorated ZnO nanocrystals: photocatalysis and charge dynamics. *ACS Applied Materials & Interfaces* **2016**, *8*, 32754-32763.
35. Pawinrat, P.; Mekasuwandumrong, O.; Panpranot, J. Synthesis of Au-ZnO and Pt-ZnO nanocomposites by one-step flame spray pyrolysis and its application for photocatalytic degradation of dyes. *Catalysis Communications* **2009**, *10*, 1380-1385.
36. Patel, J.B. Performance standards for antimicrobial susceptibility testing; twenty-fifth informational supplement. **2015**.
37. Kassim, A.; Omuse, G.; Premji, Z.; Revathi, G. Comparison of Clinical Laboratory Standards Institute and European Committee on Antimicrobial Susceptibility Testing guidelines for the interpretation of antibiotic susceptibility at a University teaching hospital in Nairobi, Kenya: a cross-sectional study. *Ann Clin Microbiol Antimicrob* **2016**, *15*, 21, doi:10.1186/s12941-016-0135-3.
38. Rietveld, H.M. A profile refinement method for nuclear and magnetic structures. *Journal of applied Crystallography* **1969**, *2*, 65-71.
39. Pecharsky, V.K.; Zavalij, P.Y. Fundamentals of Crystalline State and Crystal Lattice. *Fundamentals of Powder Diffraction and Structural Characterization of Materials* **2009**, 1-15.

40. Williamson, G.; Smallman, R. III. Dislocation densities in some annealed and cold-worked metals from measurements on the X-ray debye-scherrer spectrum. *Philosophical magazine* **1956**, *1*, 34-46.
41. Kim, K.-M.; Choi, M.-H.; Lee, J.-K.; Jeong, J.; Kim, Y.-R.; Kim, M.-K.; Paek, S.-M.; Oh, J.-M. Physicochemical properties of surface charge-modified ZnO nanoparticles with different particle sizes. *International journal of nanomedicine* **2014**, *9*, 41-56.
42. Nicholas, N.J.; Franks, G.V.; Ducker, W.A. Selective adsorption to particular crystal faces of ZnO. *Langmuir* **2012**, *28*, 7189-7196.
43. Restrepo, C.V.; Villa, C.C. Synthesis of silver nanoparticles, influence of capping agents, and dependence on size and shape: A review. *Environmental Nanotechnology, Monitoring & Management* **2021**, *15*, 100428.
44. Hessian, M.; Da'na, E.; Kawther, A.; Khalaf, M.M. Nano ZnO (hexagonal wurtzite) of different shapes under various conditions: Fabrication and characterization. *Materials Research Express* **2019**, *6*, 085057.
45. Țucureanu, V.; Munteanu, D. Enhanced optical properties of YAG: Ce yellow phosphor by modification with gold nanoparticles. *Ceramics International* **2019**, *45*, 7641-7648.
46. Fageria, P.; Gangopadhyay, S.; Pande, S. Synthesis of ZnO/Au and ZnO/Ag nanoparticles and their photocatalytic application using UV and visible light. *Rsc Advances* **2014**, *4*, 24962-24972.
47. Abdullahi, S.S.; Güner, S.; Musa, Y.; Adamu, B.I.; Abdulhamid, M.I. Simple method for the determination of band gap of a nanopowdered sample using Kubelka Munk theory. *NAMP J* **2016**, *35*, 241-246.
48. Niño-Martínez, N.; Salas Orozco, M.F.; Martínez-Castañón, G.-A.; Torres Méndez, F.; Ruiz, F. Molecular mechanisms of bacterial resistance to metal and metal oxide nanoparticles. *International journal of molecular sciences* **2019**, *20*, 2808.
49. Parvekar, P.; Palaskar, J.; Metgud, S.; Maria, R.; Dutta, S. The minimum inhibitory concentration (MIC) and minimum bactericidal concentration (MBC) of silver nanoparticles against *Staphylococcus aureus*. *Biomaterial investigations in dentistry* **2020**, *7*, 105-109.
50. Hachicho, N.; Hoffmann, P.; Ahlert, K.; Heipieper, H.J. Effect of silver nanoparticles and silver ions on growth and adaptive response mechanisms of *Pseudomonas putida* mt-2. *FEMS microbiology letters* **2014**, *355*, 71-77.
51. Regmi, C.; Joshi, B.; Ray, S.K.; Gyawali, G.; Pandey, R.P. Understanding mechanism of photocatalytic microbial decontamination of environmental wastewater. *Frontiers in chemistry* **2018**, *6*, 33.
52. Reidy, B.; Haase, A.; Luch, A.; Dawson, K.A.; Lynch, I. Mechanisms of silver nanoparticle release, transformation and toxicity: a critical review of current knowledge and recommendations for future studies and applications. *Materials* **2013**, *6*, 2295-2350.
53. Tian, E.-K.; Wang, Y.; Ren, R.; Zheng, W.; Liao, W. Gold nanoparticle: Recent progress on its antibacterial applications and mechanisms. *Journal of Nanomaterials* **2021**, *2021*, 1-18.
54. Dasari, T.S.; Zhang, Y.; Yu, H. Antibacterial activity and cytotoxicity of gold (I) and (III) ions and gold nanoparticles. *Biochemistry & pharmacology: open access* **2015**, *4*.
55. Lee, H.; Lee, D.G. Gold nanoparticles induce a reactive oxygen species-independent apoptotic pathway in *Escherichia coli*. *Colloids and Surfaces B: Biointerfaces* **2018**, *167*, 1-7.
56. Lipovsky, A.; Tzitrinovich, Z.; Friedmann, H.; Appelerot, G.; Gedanken, A.; Lubart, R. EPR study of visible light-induced ROS generation by nanoparticles of ZnO. *The Journal of Physical Chemistry C* **2009**, *113*, 15997-16001.
57. Pham, T.N.; Hue, N.T.; Lee, Y.-C.; Huy, T.Q.; Thuy, N.T.T.; Van Tuan, H.; Khi, N.T.; Phan, V.N.; Thanh, T.D.; Lam, V.D. A hybrid design of Ag-decorated ZnO on layered nanomaterials (MgAC) with photocatalytic and antibacterial dual-functional abilities. *RSC advances* **2021**, *11*, 38578-38588.
58. Banerjee, S.; Pillai, S.C.; Falaras, P.; O'shea, K.E.; Byrne, J.A.; Dionysiou, D.D. New insights into the mechanism of visible light photocatalysis. *The journal of physical chemistry letters* **2014**, *5*, 2543-2554.

Disclaimer/Publisher's Note: The statements, opinions and data contained in all publications are solely those of the individual author(s) and contributor(s) and not of MDPI and/or the editor(s). MDPI and/or the editor(s) disclaim responsibility for any injury to people or property resulting from any ideas, methods, instructions or products referred to in the content.